Enzyme and Microbial Technology 138 (2020) 109559

Contents lists available at ScienceDirect

Enzyme and Microbial Technology

journal homepage: www.elsevier.com/locate/enzmictec

Quercetin in the form of a nano-antioxidant ($QTiO_2$) provides stabilization of quercetin and maximizes its antioxidant capacity in the mouse fibroblast model

Yelda Birinci[a], Javed H. Niazi[b], Oznur Aktay-Çetin[a], Huveyda Basaga[a,*]

[a] Faculty of Engineering and Natural Sciences, Sabanci University, 34956, Tuzla, Istanbul, Turkey
[b] Nanotechnology Research and Application Center (SUNUM), Sabanci University, Tuzla, Istanbul, Turkey

ARTICLE INFO

Keywords:
Quercetin
TiO_2
ROS
Nrf2
Antioxidant therapy
Cleavages of Cas 3 and PARP

ABSTRACT

Living cells are constantly exposed to reactive oxygen species (ROS) causing them to rely on a constant supply of exogenous antioxidants. Quercetin (Q) is one of the potent exogenous antioxidants utilized in various antioxidant formulations. However, the potential application of Q is largely limited because of its poor water solubility. In this study, we employed titanium dioxide (TiO_2) nanoparticles to maximize cellular penetration and antioxidant effect of Q on mouse fibroblast cells. To accomplish this, polyethylene glycol (PEG) modified TiO_2-nanoparticle surfaces were utilized that exhibited better dispersion, with enhanced biocompatibility. Cell viability assays using Q and Q-conjugated TiO_2-nanoparticles ($QTiO_2$) were evaluated in terms of cell morphology as well as with an immunoblotting analysis to look for key biomarkers of apoptosis. In addition, cleavages of Cas 3 and PARP were obtained in cells treated with Q. Furthermore, antioxidant defence with $QTiO_2$ was validated by means of the Nrf2 upregulation pathway. We also observed increased expressions of target enzymes; HO-1, NQO1 and SOD1 in $QTiO_2$-treated cells. The antioxidant potency of the $QTiO_2$ nano-antioxidant form was successfully tested in ROS and superoxide radicals induced cells. Our results demonstrated that the $QTiO_2$ nano-antioxidant promoted a high quercetin bioavailability and stability, in cells with maximal antioxidant potency against ROS, with no signs of cytotoxicity.

1. Introduction

Oxidative stress is known for its association with a variety of diseases such as cancer, cardiovascular, neurodegenerative and age-related disorders [1]. Oxidative stress causes initiation and/or progression of these pathologies by participating actively in the cellular signalling processes. One of its important roles is linked to cell signalling, where it acts as an initiator or a repressor. Humans are continuously exposed to free radicals due to air and ground pollution, which cause oxidative stress. This causes a spontaneous struggle between cellular antioxidant defence and oxidative radicals in living cells and their survival depends on providing a balance between oxidant and antioxidant processes. Therefore, many studies have centred on exogenous antioxidant-supply from natural sources to be used for restoration of the cellular antioxidant defence. Flavonoids are one of the easily reachable antioxidant family which belong to phenolic compounds that are abundantly found in nature. The Antioxidant effects of flavonoids in cellular defence systems against reactive oxygen species (ROS) have been evidenced in a number of investigations [2]. Quercetin (Q) is one of the strongest antioxidants among the flavonoids due to its functional group carrying structure [3]. Applications of Q are ineffective because of its hydrophobicity (water solubility < 0.01 g/l), despite its efficient antioxidant potency [4]. In recent years, Q has been used in a variety of nano-formulations designed to enhance its permeability into skin cells [5]. Nanomaterials and nanoparticles have been found to be extremely beneficial in drug-delivery, and one example includes improving insoluble chemotherapeutics [6]. Because of their small size, nanoparticles have several benefits: better penetration, assured bioavailability, and a controlled drug-release. These preferable properties make them ideal carriers compared to consuetudinary drug-delivery systems. Over many years, TiO_2-nanoparticles have been widely used in paper, plastics, paints, textiles and pharmaceuticals. Applications of TiO_2 in medical fields have increased after 1990s, when it was accepted as a biologically unreactive substance [7–9]. Due to its

* Corresponding author at: Molecular Biology, Genetics and Bioengineering Program, Faculty of Engineering and Natural Sciences, Sabanci University, 34956, Tuzla, Istanbul, Turkey.
E-mail address: huveyda@sabanciuniv.edu (H. Basaga).

https://doi.org/10.1016/j.enzmictec.2020.109559
Received 8 August 2019; Received in revised form 23 March 2020; Accepted 29 March 2020
Available online 06 April 2020

high-efficiency of photoactive properties, TiO_2 has been extensively used as a major ingredient in cosmetics and sunscreen products, both of which creates a barrier against ultraviolet rays [10]. Moreover, nanoparticles of TiO_2 are among the most preferred nanoparticles, which are applied broadly in orthopaedic and dental implants, because of their antibacterial property, desired mechanical properties, and high level of biosafety [11]. As an approved biologically inert topical skin agent, TiO_2, would be suitable in a cream formulation and also served as a good nanocarrier for Q molecules in the physiological environment.

In this study, we report the formulation of a novel nano-antioxidant that utilizes Q-conjugated TiO_2-nanoparticles ($QTiO_2$) for fortifying skin defence against oxidative toxicity. Polyethylene glycol (PEG) encapsulated TiO_2-nanoparticles exhibited better dispersion and biocompatibility, which causes these PEGylated surfaces to easily adhere onto living cells. The $QTiO_2$ nano-antioxidant formulation was designed to efficiently diffuse Q molecules into the cells that are assisted by TiO_2-nanoparticles as carriers. Here, mouse fibroblast cells (Swiss 3T3 albino, ATCC, USA) were chosen as model cells because they are major cell type in mammalian connective tissue, which generates collagen and extracellular matrix (ECM) molecules and function in wound healing, tissue repair, and remodelling. The developed nanosystem was subjected to different regimes of treatment using mouse fibroblast cells as a model. Protection of $QTiO_2$ against ROS and superoxide generation was determined and validated by confocal microscope monitoring as well as by determining antioxidant capacity of the $QTiO_2$ nano-antioxidant, through the response of *Nrf2* (NF-E2 related factor 2) pathway. Our results demonstrated that Q molecules were carried by a $QTiO_2$-nanosystem that triggers *Nrf2* signalling and thus, upregulates the phase 2 enzymes, which play an important role in the antioxidative defence systems of cells. The nano-antioxidant $QTiO_2$ designed in this study enabled efficient delivery of Q molecules into mouse fibroblast cells and then strengthened cellular antioxidant defence system against oxidative toxicity.

2. Materials and methods

2.1. PEGylation of nanoparticles

Nano sized TiO_2 particles used in this study had a primary particle size of 21 nm (Sigma, cat. no: 718,467). These TiO_2-nanoparticles were surface modified with PEG-6000 (Sigma, cat. no: 81,255) according to a previous protocol [12]. TiO_2-nanoparticles were suspended in sterile distilled water and sonicated (500 W) on ice for a total of 20 min with 34 % amplitude in a 30 s pulse with 30 s intervals. The homogeneous suspension of TiO_2-nanoparticles was prepared by mixing them with PEG-6000 (1%) in a mass ratio of 1:1 (PEG: TiO_2 nanoparticles) for surface functionalization. The mixture was left overnight with constant stirring at 750 rpm at RT. The PEGylated nanoparticles were purified by centrifugation at 18,000 rpm at 10° C for 1 h, the supernatant was decanted and the pellet containing PEGylated nanoparticles were washed with distilled water. PEGylated nanoparticles obtained were freeze-dried using liquid nitrogen. The synthesized TiO_2-nanoparticles PEGylated sample was finally collected, and this sample was termed as TiO_2-nanoparticles throughout this paper.

2.2. Characterization of $QTiO_2$ and TiO_2-nanoparticles

Bare TiO_2-nanoparticles, PEGylated TiO_2-nanoparticles and Q conjugated TiO_2-nanoparticles ($QTiO_2$) were subjected to scanning electron microscopy (SEM) analysis. Control TiO_2-nanoparticles suspension in pre-PEGylation and post-PEGylation periods, and $QTiO_2$ were subjected to a 10 min ultrasonic dispersion in distilled water which yielded a homogeneous suspension. The sample was mounted on a clean silicon wafer chips followed by sputter coating of thin Pd–Au layer for SEM imaging (Cressington Sputter Au/Pd Coater). The SEM images were recorded with the help of a SEM operator at 3 keV beam (Carl Zeiss, LEO Supra 35 V P). Fourier transform infrared (FTIR) analysis of pure Q, $QTiO_2$ and bare/PEGylated TiO_2-nanoparticles were carried out using a Nicolet iS10 FTIR spectrometer at the range of $1000-4000\ cm^{-1}$. Fluorescence spectra of (i) $QTiO_2$ conjugates, (ii) PEGylated TiO_2-nanoparticles, and (iii) pure Q were recorded using a Nanodrop 3300 Fluorospectrometer with a white LED excitation.

2.3. Q conjugation to PEGylated TiO_2-nanoparticles

The concentration of Q (Applichem, cat. no: A3415) was measured at its characteristic maximum absorption wavelength of 255 nm. The Q conjugation with PEGylated TiO_2-nanoparticles was performed by incubating them with the Q suspension in a mass ratio of 1:1, under constant stirring overnight at RT. This Q suspension was centrifuged at 2000 rpm for 5 min at RT and the residual Q in the supernatant was measured spectrophotometrically. Following this, the pellet collected was re-suspended and washed in the same volume of 1X PBS (Fig. S1).

The % Q conjugation was calculated based on the relative concentration difference before and after the conjugation process by Eq. (1) as follows:

$$\text{Drug conjugation } \% = [(A-B)/A] \times 100 \quad (1)$$

Where 'A' and 'B' indicate the Q concentration, before and after conjugation, respectively.

2.4. Cellular uptake of Q and $QTiO_2$

Cellular uptake of Q and $QTiO_2$ were examined under a laser scanning confocal microscope (Carl Zeiss, LSM 710) with 63X objective. Visualisation of Q in the mouse fibroblast cells was determined with the help of fluorescence properties of [13,14]. Cells were seeded onto glass slides in the multi-well plates and and grown in a humidified chamber (37 °C and 5 % CO_2). Cells were treated with Q and $QTiO_2$ for different time intervals (1, 3, 6, 12 and 24 h). After treatments, the cells were fixed on slides with 4 % paraformaldehyde (PFA) for 10 min at RT. The slides were quickly covered with a cover-slip with the aid of the mounting solution (ThermoFisher, cat. no: S36972) containing dapi dye. Cells were then monitored using a confocal microscope with an Ex/Em: 488/520 nm filter set, compatible with Q.

2.5. Cell-culturing and treatment conditions

The mouse fibroblast cells (Swiss 3T3 albino, ATCC, USA) were used in this study because they are the most common cells of connective tissue. Mouse fibroblast cells were grown in DMEM medium and subcultured when the confluence reached to about 80 %. These cells were later split into experimental groups for the following treatment regimens: (i) quercetin-conjugated TiO_2-nanoparticles ($QTiO_2$)-treated cells; (ii) quercetin (Q)-treated cells only; and (iii) PEGylated TiO_2-nanoparticles (TiO_2)-treated cells only. For the control groups, untreated cells were used under identical test conditions, while in all other regimes, $QTiO_2$ nano-antioxidants were amended in cell-culture media whose final concentration was adjusted to $100\ \mu g\ ml^{-1}$..

2.6. Cellular viability evaluation

Cell viability assays were performed using a commercial kit (Sigma-Aldrich, cat. no: 11644807001) following the steps recommended in the manufacturer's instructions. The cells were cultured in 96-well microtitre plates (final volume of 100 µL/well) until reaching a seeding-density of 5×10^4 cells/well followed by treating cells with 10 µL WST-1 reagent (supplied with the kit) to each reaction and the plates were incubated for 4 h at 37 °C. The absorbances at 450 nm and 655 nm were measured against the control background (blank) and the reference samples, respectively using a microplate reader (Bio-rad iMark, USA).

The results obtained were calculated as the percent cell viability with respect to the control that represents 100 %.

2.7. Total ROS and superoxide assessments

Total cellular ROS was measured using a commercial kit (Abcam, cat. no: ab139476). Cells were grown to a seeding density of 5×10^4 cells/well in a black 96-well microtitre plate (final volume of 100 µL/well). ROS or superoxide generation was triggered by incubating cells with a ROS inducer, 50 µM Pyocyanin (PCN), for 45 min at 37 °C in dark conditions. The final concentration of PCN was determined experimentally for mouse fibroblast cell as indicated in Fig. S2. The ROS generation was inhibited 30 min prior to ROS induction by addition 5 mM of NAC (*N*-acetyl-*L*-cysteine), a ROS inhibitor, which served as a negative control as per the manufacturer's instruction. ROS/superoxide generation was measured in a microplate reader (Molecular Devices, SPECTRAmax GEMINIxps) by recording the fluorescence after adding the supplied reagent with the kit. The reader was equipped with a filter set compatible with fluorescein (Ex-Em: 488 − 520 nm) and rhodamine (Ex-Em: 550 − 610 nm).

2.8. Protein isolation and immunoblotting

Total protein was isolated after harvesting cells by spinning them at 1214 rpm for 5 min and the cells were re-suspended in ice-cold PBS. The cell-suspension was again centrifuged for 30 s at 13,200 rpm and the cell-pellet was lysed after 30 min of incubation, in a buffer containing phosphatase and protease inhibitors for total cell-lysis. The cell-lysate was again centrifuged at 13,200 rpm for 10 min and the supernatant was collected as a total cell-free protein extract and placed in a − 80 °C freezer until use. Concentrations of protein were determined by the Bradford method using a commercial kit (Bio-Rad, cat. no: 500-0201). The isolated protein-fractions were disassociated on 12–15 % SDS-polyacrylamide gel electrophoresis (PAGE) followed by transferring onto polyvinylidene difluoride (PVDF)-membrane (Amersham Pharmacia Biotech, cat. no: 10,600,023). The PVDF-membranes were later submerged in a solution of 5% non-fat dry milk, in PBS-Tween20, and this was incubated overnight with primary antibodies. After incubation, PVDF-membranes again were washed with PBS-Tween20, and then incubated with a secondary antibody conjugated with HRP and washed with PBS-Tween20. The proteins were then analysed with an ECL Advance (GE, cat. no: RPN2209) and exposed to a Hyperfilm-ECL (GE, cat. no: 28,906,836). The following primary antibodies used in this study that were acquired from Cell Signaling Tech. Inc. (Beverly, MA, USA) and these are; Caspase 3 (CST, cat. no: 9662), cleaved caspase 3 (CST, cat. no: 9664), PARP (CST, cat. no: 9542), Nrf2 (CST, cat. no: 12,721), SOD1 (CST, cat. no: 2770), NQO1(CST, cat. no: 42,672), HO-1 (CST, cat. no: 5061), and Beta-actin (CST, cat. no: 4967). The antibodies were used with a 1000-fold dilution for immunoblotting. Anti-rabbit (CST, cat. no: 7074) and anti-mouse (CST, cat. no: 7076) secondary HRP-conjugated antibodies were used with a 5000-fold dilution for immunoblotting in which. In order to standardize protein-loading, Beta-actin was used as a control protein and the protein amount was determined by densitometry method. For data quantification, the intensity of protein bands was analysed using ImageJ software and all data were validated with band intensities with respect to the Beta-actin.

2.9. RNA isolation and quantitative real-time PCR (qRT-PCR)

Cells were seeded on 60 mm tissue culture plates and treated with Q and $QTiO_2$. After washing with sterile PBS, the cells were removed and harvested by spinning for 5 min at 300 *g*. Total RNA was isolated using a commercial RNA isolation kit (Qiagen, cat. no: 217004) according to the manufacturer's protocol. Total RNA concentrations and the A_{260}/A_{280} ratio were determined spectrophotometrically using a NanoDrop 2000 (Thermo Fisher). QuantiTect SYBR Green RT-PCR Kit (Qiagen, cat. no: 204243) was used to quantify *Nrf-2* gene expression. PCR was performed according to the manufacturer's protocol. Briefly, master mixes were prepared for *Nrf-2* (Qiagen, cat. no: QT00095270) and *Beta-actin* (Qiagen, cat. no: QT00095431) with primers that were purchased from QuantiTect Primer Assays. cDNA synthesis and amplification of the genes of interests were quantified using a thermocycler (Roche, LightCycler 480) with initial 50 °C for 30 min, 95 °C for 15 min and 40 cycles of 94 °C for 15 s and 55 °C for 30 s and 72 °C for 30 s according to the miScript SYBR Green RT-PCR Kit protocol. Data acquisition was performed at the end of each extension step. Obtained C_T values of target genes were normalized to the expression of the housekeeping gene *Beta-actin,* and the relative fold change was quantified by using the $2^{-\Delta\Delta CT}$ method [15].

2.10. Nrf2 immunostaining and nucleus colocalization analysis

Cells were seeded on coverslips (Jena Bioscience circular cover slide (22 mm), CSL-104) and grown in a humidified chamber (37 °C and 5 % CO_2). Following $QTiO_2$ treatments, the cells were fixed with 4 % PFA (paraformaldehyde) for 10 min at RT and washed thrice with PBS and permeabilized membrane with 0.05 % Triton X-100, and after the required washes, the cells were incubated with 0.1 % BSA (blocking solution) for 30 min at RT. The anti-Nrf-2 antibody was 1:400 diluted in a blocking solution, and cells were incubated with the Nrf-2 antibody overnight at + 4 °C. The next day, the cells were washed thrice with PBS and incubated with the Alexa Fluor-488 antibody (Thermo Fisher Scientific, cat. no: A-11029) in dark for 1 h and the cell nuclei was stained with dapi dye (Life Technologies, cat no: D1306). The cells were mounted on glass slides (0.17 mm, Thermo Fisher Scientific) and examined with a laser scanning confocal microscope (Carl Zeiss, LSM 710) with a 63X objective. The post-processing of visualized cells was performed in ZEN Blue software. Nrf-2 and nucleus colocalization was analysed using CoLocalizer Pro 3.0.2 software. Colocalization of two channels (blue-green) was evaluated with an algorithm which calculates the signal intensity of pixels [16]. The colocalization analysis revealed a Manders' overlap coefficient, and these coefficient values were quantified and statistically tested.

2.11. Laser scanning confocal microscope examination

Cells were seeded onto glass slides in the multi-well plates and observed by using a laser scanning confocal microscope (Carl Zeiss, LSM 710) with a 20X objective. Both PCN and NAC were used as an inducer and inhibitor of ROS, respectively. Cells were incubated for 1 h at 37 °C after adding ROS detection reagent, then washed with washing buffer and fixed onto a slide by incubating for 10 min with a 4 % PFA solution, under the dark conditions. The cells fixed on slides were quickly covered with a cover-slip with the aid of the mounting solution (ThermoFisher, cat. no: S36972) containing dapi dye. The slides were observed using a laser scanning confocal microscope with an Ex/Em: 488/520 nm filter set specific for fluorescein.

Confocal images were recorded with the software, ImageJ after applying the Corrected Total Cell Fluorescence (CTCF) computation to measure fluorescence intensity. The values of CTCF were quantified using the following Eq.2:

CTCF = integrated density– (selected cell area X mean background fluorescence). (2)

Each CTCF-value was divided-by the cell-numbers counted in the respective image. Cells were then counted by the option of particle analysis option in the ImageJ software and rounded off number to 100 cells.

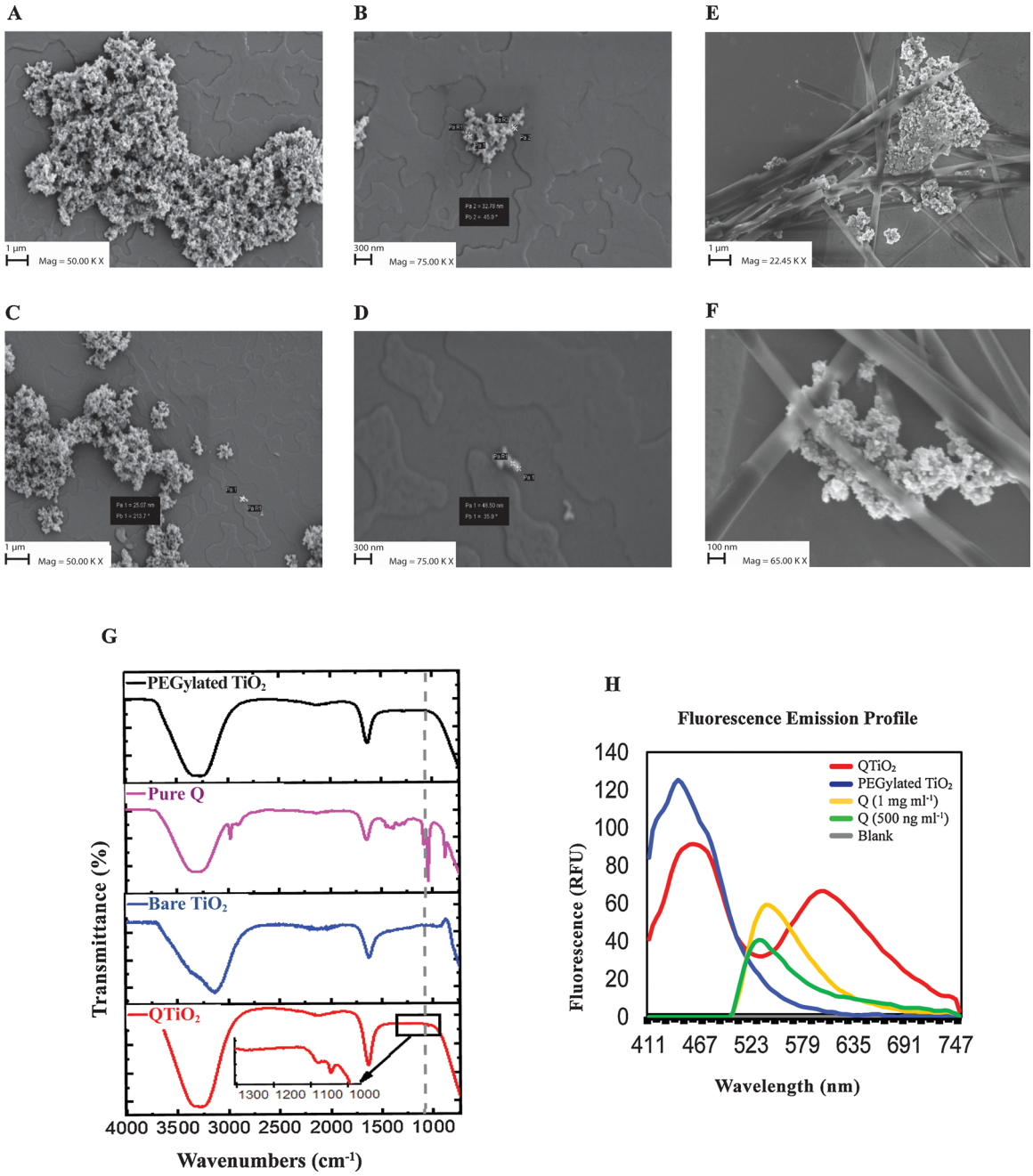

Fig. 1. Characterization of $QTiO_2$.
(A) Bare TiO_2-nanoparticles display an accumulation behavior and form cumulus before PEGylation. **(B)** TiO_2-nanoparticles display a nano size range of ~33 nm on average in SEM imaging. **(C)** After PEGylation, TiO_2-nanoparticles indicate reasonably dispersion compared to those of bare TiO_2-nanoparticles. **(D)** The approximate size of TiO_2-nanoparticles as obtained from SEM analysis to be ~50 nm. **(E)** The SEM images at 22.45 KX and **(F)** 65.000 KX magnification of $QTiO_2$ after Q conjugation. **(G)** FTIR spectra of; control PEGylated TiO_2-nanoparticles, control pure Q, control bare TiO_2-nanoparticles and test $QTiO_2$. The inset figure in ($QTiO_2$) shows a magnified portion of spectra showing peaks corresponding to Q. **(H)** Fluorescence emission spectra of control PEGylated TiO_2-nanoparticles and pure Q and comparison with $QTiO_2$ after Q conjugation. The conjugation of Q with PEGylated TiO_2-nanoparticles resulted a red-shift in fluorescence peak of Q indicating chemical conjugation.

2.12. Statistical analysis

All *in vitro* experiments were carried out with at least three independent replicates, while for western blotting assays, a minimum of two trials were conducted. All data were presented as means ± SE (standard error of derived from mean). A student's *t*-test was performed to analyze the data.

3. Results

3.1. Characterization of $QTiO_2$

The morphology of TiO_2-nanoparticles was examined by SEM imaging in which the bare TiO_2-nanoparticles (before PEGylation) indicated that they tend to agglomerate over time in spite of their extensive ultrasonic homogenization which could be associated with inherent physicochemical properties of the TiO_2-nanoparticles (Fig. 1A,

B). TiO_2-nanoparticles after PEGylation appeared to have dispersed moderately as compared to those of the control nanoparticles without PEGylation and display an avarage nano size range of $\sim 25-50$ nm, providing a large relative surface-area (Fig. 1C, D). These PEGylated TiO_2-nanoparticles served as efficient carriers of quercetin that was experimentally calculated according to Eq. 1 to be > 95 % of the conjugation capacity, which finally yields as a $QTiO_2$ complex (Fig. 1E, F).

FTIR analysis was carried out with controls such as bare TiO_2-nanoparticles, PEGylated TiO_2-nanoparticles, pure Q and compared with that of test $QTiO_2$ sample. The results are shown in Fig. 1G. FTIR spectra of $QTiO_2$ exhibited strong broad bands at $3200-3400\ cm^{-1}$ and $1700-1600\ cm^{-1}$ regions similar to the samples of pure Q and PEGylated TiO_2-nanoparticles that indicated intermolecular chemical interactions. The peaks at $1150-1070\ cm^{-1}$ region that corresponded well with the FTIR spectra of pure Q (Fig. 1G and inset) and similar results were previously reported for Q-conjugated superparamagnetic iron oxide nanoparticles [17]. Fluorescence emission spectra of $QTiO_2$ showed an emergence of a new peak when compared to spectra of control pure Q and PEGylated TiO_2-nanoparticles (Fig. 1H). This new peak can be attributed due to the presence of Q conjugation within the $QTiO_2$ matrix. However, we observed that the new fluorescence peak emerged was not identical to that of pure Q peak. We speculate that the peak emerged post-conjugation with Q in $QTiO_2$ tended to red-shit by 80 nm (from 525 nm to 605 nm) (Fig. 1H). This shift in Q emission peak from $QTiO_2$ may be due to the chemical conjugation within the PEG-matrix of the $QTiO_2$ conjugates. The concentration of Q within $QTiO_2$ conjugates was therefore determined by taking into account of the red-shift fluorescence intensity (relative fluorescence unit, RFU) at 605 nm, which was calculated to be $1\ mg\ ml^{-1}$.

3.2. Cellular uptake of Q and $QTiO_2$

Mouse fibroblast cells were incubated with Q and $QTiO_2$ at different time intervals (1, 3, 6, 12 and 24 h) and the cellular penetrations were observed under the confocal microscope. The untreated cells were used as control groups and represented as the 0 h as shown in the Fig. 2, in which the merged images included cell nuclei and Q with blue and green colors, respectively. Only nuclei stained cells are shown on the lower-right side of each image. The data indicate that Q and $QTiO_2$ penetrate the cells efficiently and both are localized mostly in the cytoplasmic compartments of the cells. However, intracellular distributions of $QTiO_2$ molecules are homogenous and do not change considerably over 24 h compared to Q molecules. It can be concluded that Q molecules are stable inside of the cell by the form of $QTiO_2$ nano-antioxidant.

3.3. Q and $QTiO_2$ effects on cell viability

Testing cell viability was performed using cells treated with two concentrations of $QTiO_2$ nano-antioxidant (100 and $250\ \mu g\ ml^{-1}$) and its components for 24 and 48 h along with respective control groups. After 24 h of exposure of $100\ \mu g\ ml^{-1}$ $QTiO_2$ doses, cells exhibited a moderate change in cell viability, however, Q-treated cells exhibited only 53 % cell viability compared to that of control cells (Fig. 3A). When cells were exposed to higher $QTiO_2$ doses ($250\ \mu g\ ml^{-1}$), it revealed a 14 % reduction in cell viability, while Q-treated cells tended to lose 92 % cell viability as compared with the untreated cells. Except for the $QTiO_2$-treated cell group, extending the duration of exposure to 48 h resulted in a sharp decline in cell viability (Fig. 3A). Based on the above results, it is concluded that the $100\ \mu g\ ml^{-1}$ of $QTiO_2$ dose at 24 h exposure found to be an optimum condition for the cells, and this condition was used for all subsequent experiments.

For an in-depth analysis of induced cell death, expressions of critical proteins such as those of apoptosis-signalling pathways were studied. Here, apoptotic proteins, such as caspase 3 (Cas 3) and poly (ADP-ribose) polymerase (PARP) were examined in experimental groups that were pre-treated with $QTiO_2$, Q, and TiO_2 for 24 and 48 h, respectively. Results of this experiment showed no significant difference among the groups with respect to apoptotic protein levels (Fig. 3B). However, the Q-treated groups (24 and 48 h) contained insufficient amounts of protein due to cell death which validates the results of the viability assays as shown in Fig. 3A. Subsequently, the existence of apoptotic markers was investigated for earlier treatment times. The data demonstrated Cas 3 and PARP cleavages occurred in Q-treated groups at 6 and 12 h treatment time intervals (Fig. 3C, D). These results were also consistent to the apparent physical alterations observed in cells suggesting cell death, which had occured in Q-treated cells after 6 and 12 h of treatment (Fig. 3E).

3.4. Expression of Nrf2 and its target enzymes

A key *Nrf2* gene is expressed during oxidative stress conditions for cell-survival. For the investigation of $QTiO_2$ nano-antioxidant potency, we focused on the *Nrf2* pathway. First, the Nrf2 protein migration from the cytoplasm to the nucleus in order to activate its target genes was monitored by Nrf2 immunostaining for 24 h (Fig. 4A). Colocalization analysis demonstrated that the Nrf2 migration began after 3 h of treatment and reached a maximum level in the 12th hour (Fig. 4B). Then, Nrf2 protein expression was observed by western blotting samples treated for 24 and 48 h among experimental groups, where the results showed no remarkable difference in the Nrf2 protein expression levels (Fig. 5A). Q-treated cells group did not yield sufficient protein

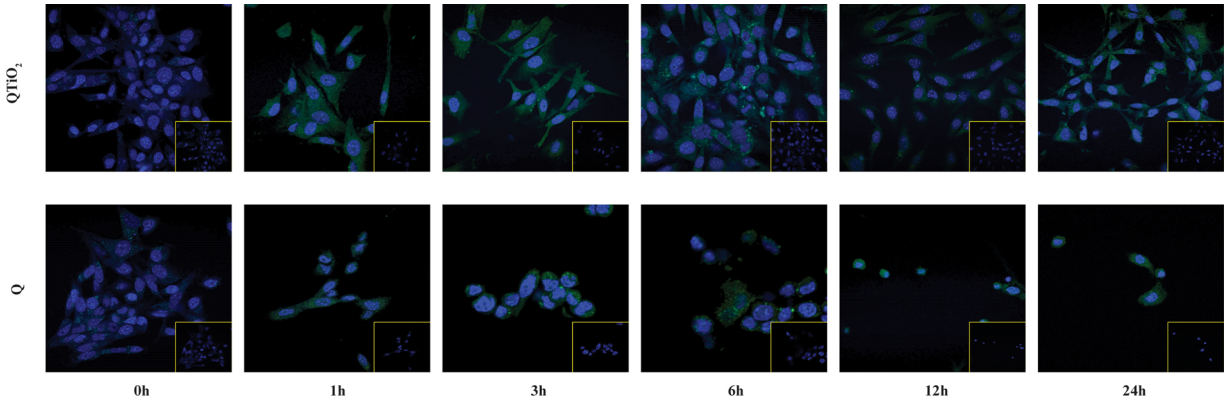

Fig. 2. Cellular uptake of Q and $QTiO_2$.
Monitoring cellular internationalization of Q and $QTiO_2$ under the laser scanning confocal microscope after treatments. The cells were treated with Q and $QTiO_2$ for 1, 3, 6, 12 and 24 h. Untreated control cells are represented with 0 h in the images. The merged images are shown cell nuclei and intracellular Q with blue and green colors, respectively. Solo dapi dyed images are shown on the lower-right side of each image.

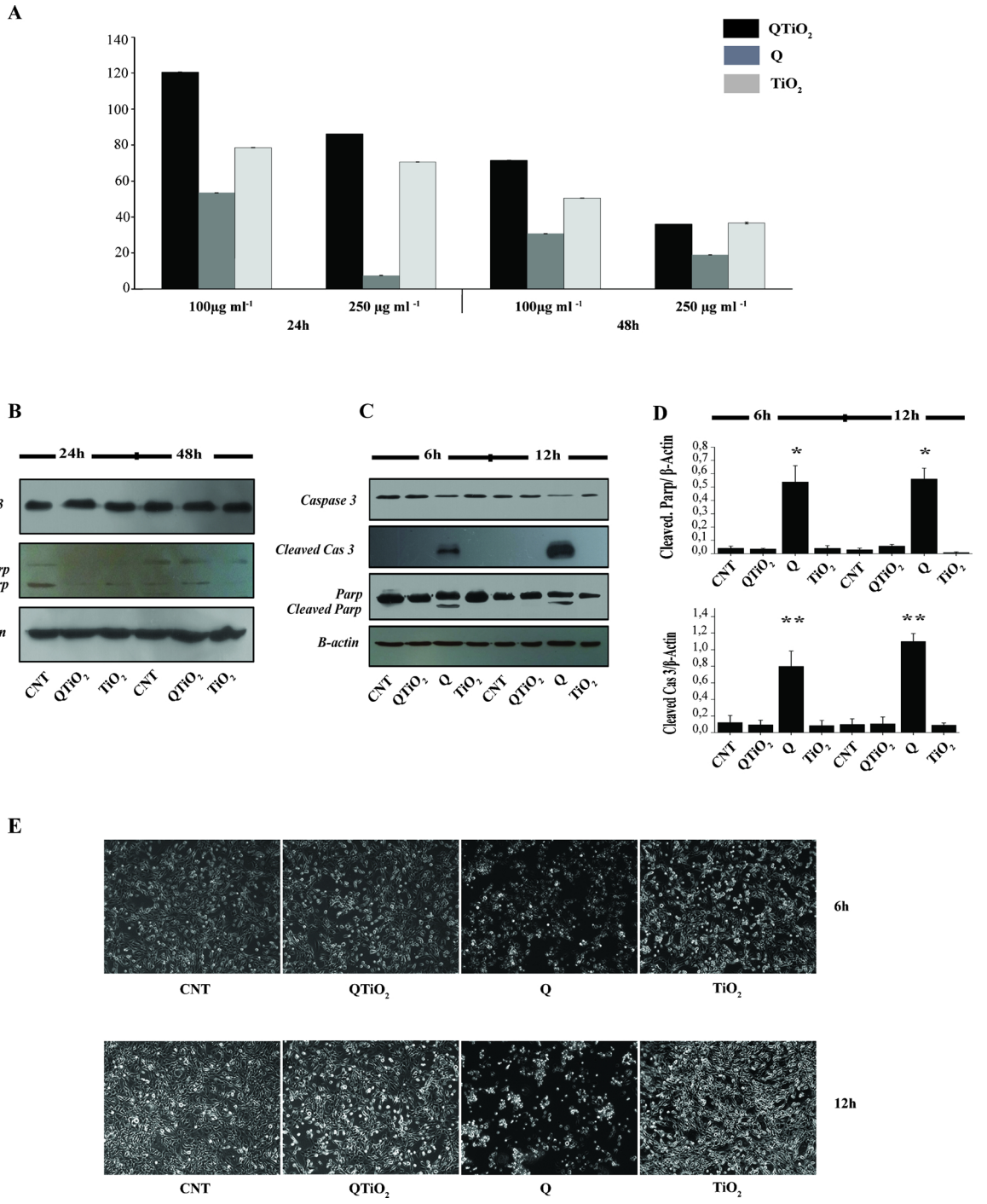

Fig. 3. Cell viability assessments.
(A) Viability assays were performed by the treatments of $QTiO_2$, Q, and TiO_2-nanoparticles on cells for 24/48 h time periods with two doses (100 µg $ml^{-1}$and 250 µg ml^{-1}). The viability values were compared to the untreated control cells and given as a percentage. Data state the mean results ± SEM, $n = 3$. **(B)** Western blotting analyses of Cas 3 and PARP proteins at 24 and 48 h periods after treatment. **(C)** Cleavages of Cas 3 and PARP proteins were clearly shown in Q-treated cells at 6 and 12 h of treatment. **(D)** Graphs state the mean values ± SEM, $n = 2$; densitometric measurements were normalized against the corresponding Beta-actin levels and asterisks indicate significant changes (*$P < 0.001$ and **$P < 0.05$) vs. control. **(E)** The pictures display morphologic alterations on cells in the earlier times of treatment (6 and 12 h). Imaging was done by using a Zeiss AxioVert Inverted Microscope with 10X objective. The cell numbers in Q-treated groups sharply declined with time and shown morphologic changes like cell detachment and clumping. The viability test results of 6 and 12 h treatment can be checked in supplementary data (Fig. S3)

content required immunoblotting analysis and therefore, Nrf2 expression was examined at early treatment times with $QTiO_2$ and Q. The Nrf2 expression was induced by $QTiO_2$ during 6 and 12 h of exposure that tended to increase with time as evidenced by densitometry analysis (Fig. 5B) and this trend corresponded to the results of Nrf2 immunostaining analysis (Fig. 4B). Further, *Nrf2* gene expression at short duration of cell exposure with Q and $QTiO_2$ was also investigated by qRT-PCR. The results revealed a significant increase with 6 and 12 h treatment of $QTiO_2$, which is consistent with immunoblotting analysis (Fig. 5D). We later examined downstream genes of *Nrf2*, which codes

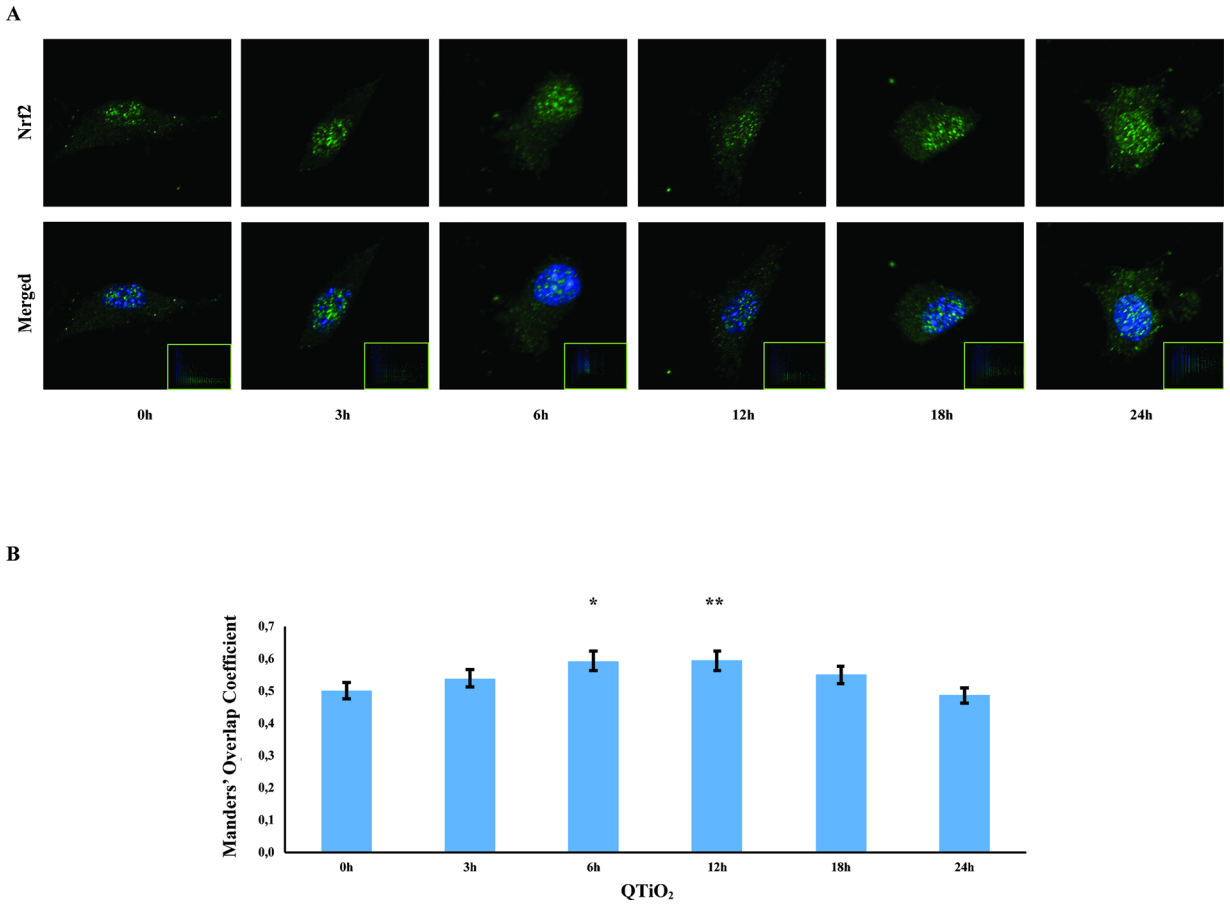

Fig. 4. Nrf2-nucleus colocalization with $QTiO_2$ treatment.
After cells are treated with $QTiO_2$ at indicated time periods, immunostaining was performed by using Nrf2 antibody and visualized by a laser scanning confocal microscope. Nucleus staining with dapi is shown in blue channel. Nrf2 is detected with Alexa Fluor 488 conjugated secondary antibody and represented in green channel. 0 h indicates control condition. **(B)** The colocalization analysis of Nrf2 protein and nucleus was done by using CoLocalizer Pro software. Pixel scattergram of green and blue channels are shown on the lower-left part of each image. Histograms represent the mean values ± SEM of minimum three independent experiments. Asterisks indicate significant changes (*$P < 0.05$ and **$P < 0.005$) vs. control.

for an antioxidative enzyme of cytoprotective significance, mainly HO-1 (heme oxygenase-1), NQO1 (NAD(P)H: quinone-oxydoreductase 1) and SOD1 (superoxide dismutase1), by immunoblotting. $QTiO_2$-treated cells showed increased levels of the HO-1 enzyme after the 12 h of treatment interval according to densitometry (Fig. 5C). However, Q-treated cells showed only a mild increase in HO-1 expression after 6 h of treatment which disappeared post 12 h treatment interval. Higher NQO1 enzyme expression was found in $QTiO_2$-treated cell groups at both treatment intervals (6 and 12 h), compared to Q-treated cell groups (Fig. 5C). SOD1 levels remained relatively constant or rose in each of tested experimental groups, except Q-treated cells (Fig. 5C). It is clear from the above results that increased levels of Nrf2 protein expression occurred only in the pre-treated cells with $QTiO_2$, but not with Q alone.

3.5. Total ROS and superoxide determination

The PCN-treated cells group that exhibited the highest amount of ROS used as a reference positive control group in this study (Fig. 6A). ROS production was fully prevented in cells treated with $QTiO_2$ (> 100 %) and this result was comparable to detected in reference negative control cells (NAC-treated cells). While a minimum level of ROS generation was observed in Q-treated cell group, and higher level in the TiO_2-treated group. The above trend seen in ROS measurements corresponded well with the measured superoxide levels in the same cell groups (Fig. 6B). The $QTiO_2$-treated cell group showed a significant reduction in both ROS and superoxide levels suggesting that the $QTiO_2$ prevents the generation of superoxide/ROS species efficiently. The Q-treated group, however, showed a minimum level of superoxide production, but the $QTiO_2$ nano-antioxidant treatment exerted a lasting high level of cell protection against ROS and superoxide generation.

3.6. Confocal microscopic examination of ROS in cells

Results of total cellular ROS analysis were validated by confocal microscopy. Cell nuclei dyed with dapi and green fluorescence in confocal images indicated the presence of ROS (Fig. 7A, B). The highest fluorescence intensity was detected in PCN-treated cell group, followed by TiO_2-treated group. The fluorescence intensity with $QTiO_2$ and NAC treatments appeared at similar intensity levels suggesting that these groups have similar antioxidant protection (Fig. 7C). The confocal assay using dapi dyed cells revealed consistent trend with that observed from quantitative ROS measurement (Fig. 6A). The results showed that there was a significant reduction of ROS activity in $QTiO_2$-treated cells, which was evident in both captured images and the quantitative evaluation.

4. Discussion

A good method for enhancing the cellular antioxidant defence system is by using exogenous antioxidants, which prevent oxidative toxicity and restore normal cellular activity. Quercetin, a flavonoid molecule is known for its high level of antioxidant activities, which

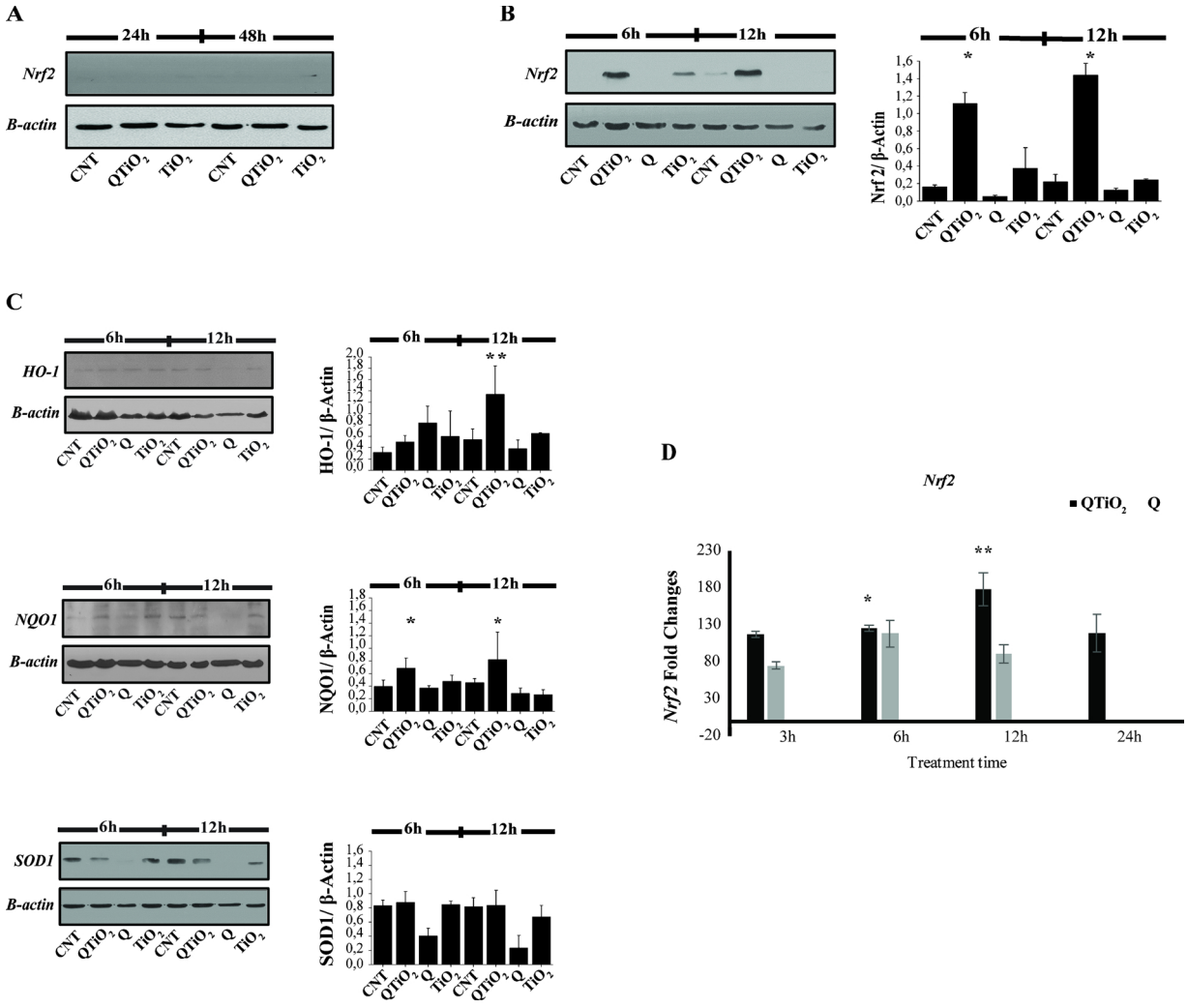

Fig. 5. Expression of Nrf2 and its target enzymes.
(A) It was not observed any differences in expressions of Nrf2 protein during the treatment time periods whereas Nrf2 levels risen importantly in $QTiO_2$-treated groups by time as shown in Figure **B**. **(C)** $QTiO_2$ time and dose dependently induced HO-1 and NQO1 expressions considerably according to densitometric analysis. *SOD1* enzyme level increased slightly in $QTiO_2$-treated groups. Histograms represent the mean values ± SEM of minimum two independent experiments; densitometric analyses were normalized against corresponding Beta-actin levels. Asterisks indicate significant changes (*P < 0.05 and **P < 0.005) vs. control. **(D)** *Nrf2* gene expressions significantly increased by the time in $QTiO_2$-treated groups by showing a similar trend with Nrf2 protein levels. Q-treated cells did not show a significant change in gene expression and protein levels about Nrf2 pathway. qRT-PCR results represent the mean values ± SEM of minimum three independent experiments. Control was taken as a 100 % and significant differences as represent *P < 0.05 and **P < 0.005 vs. control.

come from its abilities such as scavenging of reactive species, inhibiting lipid-peroxidation, and chelating metal ions [18,19]. Nevertheless, utilization of Q is limited largely due to its hydrophobicity and yet Q has been designed in different kinds of nano-formulations, like glycerosomes and deformable-liposomes to address its low water solubility and increase its stabilization [5]. Despite these nano-formulations they have ameliorated Q's function compared to the pure form in terms of diffusing through skin, consequently the optimized formula is yet to be developed [20,21]. In this study, we conjugated Q to TiO_2-nanoparticles in order to enhance the efficiency of Q delivery. To accomplish this, TiO_2-nanoparticles were first surface modified using PEG to yield more adhesive and biocompatible forms of nanoparticles. PEGylated forms of TiO_2-nanoparticles achieved a maximum conjugation ratio of Q (> 95 %) resulting in a more feasible in Q-delivery into cells. It has been demonstrated that agglomeration of TiO_2-nanoparticles can be minimized through PEGylation which ensure a homogenously dispersing in suspension compared to their counterpart non-PEGylated nanoparticles (Fig. 1C). A better antioxidant function of Q is dependent upon cellular penetrance efficiency. As shown in Fig. 2, Q penetrates into cells efficiently in the form of the $QTiO_2$ nano-antioxidants and remain stable in the cell as well.

$QTiO_2$-treated mouse fibroblast cells were analysed for their viability and compared to respective controls. It was observed that the cells remained unaffected 24 h after treatment with 100 μg ml^{-1} of $QTiO_2$ nano-antioxidants, and these were similar to those of untreated cells. Contrastingly, cells treated with the same concentration of Q resulted in a dramatic loss in the cell population (Fig. 3A). However, after 48 h of treatment, cell viability tends to drastically decline in all cell groups except with $QTiO_2$-treated cells. Further increase in concentration to 250 μg ml^{-1} proved to be toxic to only Q-treated cells, while $QTiO_2$-treated cells exhibited just a moderate reduction in cell viability. In other words, $QTiO_2$-treated cells were able to sustain viability greater than that of Q-treated cells (Fig. 3A). This data is consistent with previous reports showing decreasing viability of cells after their exposure to TiO_2-nanoparticles [22–24]. As shown in Fig. 3E, the morphologic examination of $QTiO_2$/Q-treated cells after 6 and 12 h treatment times are also consistent with their viability profile (Fig. S3). Flavonoids have shown to possess pro-oxidant efficacy at high amounts [25,26], and

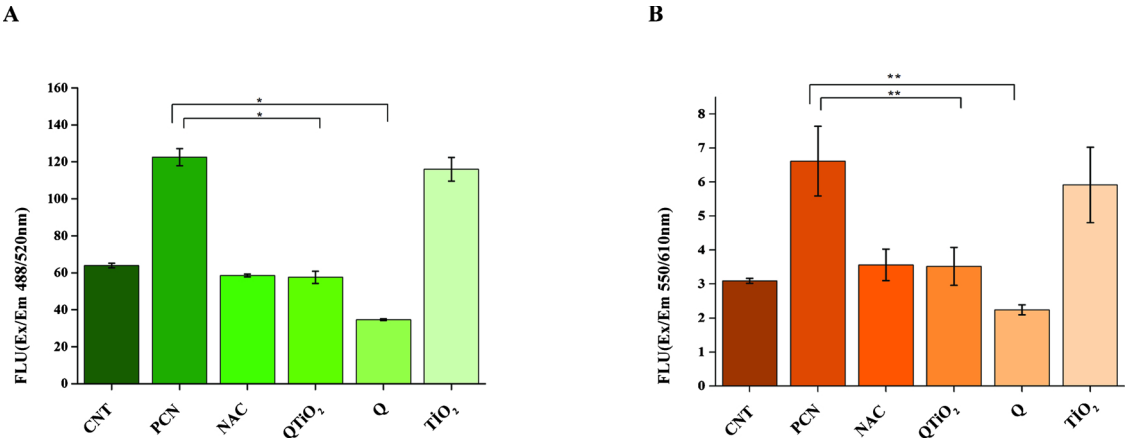

Fig. 6. Total ROS and superoxide determination.
Measurements were done in fluorescence microplate reader with a filter set compatible with fluorescein (Ex-Em:488 − 520 nm) and rhodamine (Ex-Em:550 − 610 nm) according to the manufacturer's kit protocol. PCN and NAC were used as inducer and inhibitor of ROS, respectively. Measurements of total ROS **(A)** and Superoxide **(B)** showed the similar trend for all groups. Data shown in figures state the mean results ± SEM, results from 3 independent experiments. Asterisks represent important differences among experimental groups (*P < 0.005 and **P < 0.05).

resulting toxicity is associated with their hydroxyl groups [27]. Also, Q has been regarded as mutagen and therefore, it can exhibit cytotoxic effects [28,29]. It is apparent that loss in viability of Q-treated cells has been observed in the early treatment intervals and this then tend to decline with exposure time (Fig. 3A).

Apoptosis is a programmed cell death, which occurs via 2 signalling pathways and these are named as an intrinsic (mitochondrial) and an extrinsic (via death receptor) pathway [30]. Activation of a proteolytic caspase cascade is a common process that exists in both apoptotic pathways. This activation causes cleavages of the effector cas-3, 6 or 7 as further steps in the pathway [31]. The underlying molecular mechanism of Q cytotoxicity in this study was analysed by immunoblotting of key proteins related to apoptosis. Cleavages of Cas 3 and PARP proteins are two major processes that occurred which are possibly linked to apoptosis, and we found evidence of this in Q-treated cell groups at 6 and 12 h (Fig. 3C, D). Cas 3 is the widespread executioner caspase [32] and extinguishes the cell by PARP cleavage [33]. Our data evidently showed that the Cas 3 dependent apoptotic pathway was activated by Q in mouse fibroblast cells (Fig. 3C). Previous studies also showed that Q induced apoptosis by caspases activation in human breast cancer cells [34]. In another report, varying Q amounts were utilized to hepatic stellate cells which showed Cas 3 and PARP1 cleavages, and this property is consistent with what was observed in this study (Fig. 3C), where both Cas 3 and PARP1 were upregulated in a dose-dependent manner by Q [35]. This is a confirmation that 100 μg ml^{-1} of Q causes apoptotic cell death, but an equal amount of Q, if it is in the form of conjugated TiO_2-nanoparticles, did not activate this pathway.

The pro-oxidant effect is also considered to be responsible for the flavonoids' cytotoxic and pro-apoptotic effects [18]. The antioxidant feature of Q can be shifted to its pro-oxidant property, depending upon its level, and oxidative sources [36]. Further, activation of the Nrf2 pathway by an agent like a pro-oxidant is necessary for maintaining cellular redox homeostasis in normal physiological conditions [37]. The pro-oxidant can react with keap1 (Kelch-like ECH-associated protein 1) and oxidize its sulfhydryl group, thus, causing Nrf2 disassociation from keap1. Following this, Nrf2 moves into the nucleus and stimulates expression of phase II antioxidant enzymes. In this study, we tested the $QTiO_2$ and pure Q effects on the Nrf2 pathway, respectively. We found out that the Nrf2 proteins are located in nucleus and their nuclear accumulation increase with $QTiO_2$ 6 and 12 h of treatment according to colocalization analysis (Fig. 4). Further, we show that $QTiO_2$ induced the *Nrf2* gene (Fig. 5D) and hence its protein expression over time (Fig. 5B). Moreover, HO-1 and NQO1 levels rose in $QTiO_2$-treated cells at the 12 h of treatment (Fig. 5C). Taken together, there was a moderate rise in SOD1 expressions in the $QTiO_2$-treated cells and this was shown in the densitometry analysis (Fig. 5C). However, Nrf2 expression did not show a significant change in Q-treated groups, with both protein and gene levels (Fig. 5B, D). While the highest levels of the Nrf2 target enzymes were detected in $QTiO_2$-treated cells and Q-treated cells exhibited least expressions of the same enzymes. This can be explained that a high concentration of Q is toxic for the cells and therefore the cells undergo programmed cell death. The apoptotic signals seen in these groups are clear evidence of this phenomena (Fig. 3C). Based on this result, it can be suggested that the $QTiO_2$ nano-antioxidants inhibit cellular death by triggering Nrf2 signalling which is a survival mechanism (Fig. 8).

TiO_2-nanoparticles at high levels have been demonstrated to cause cell death in many types of cells. For instance, PARP cleavage triggered by TiO_2-nanoparticles was observed in phytohemagglutinin-stimulated human lymphocytes over the course of 24 h [38]. However, in our study, we have not detected any apoptotic alterations in TiO_2-treated cell groups (Fig. 3D). The inconsistency in results compared with previous reports can be attributed to use of surface modified TiO_2-nanoparticles (PEGylated-TiO_2-nanoparticles) rather than bare TiO_2-nanoparticles, which suppressed the cytotoxic effects of the bare form.

Stability in physiological conditions of a molecule is governed by its functionality. Therefore, here we aimed to conjugate a high amount of quercetin by means of surface functionalization using a PEG-layer on nanoparticles which provided more stability if they were brought to close proximity of the cells. Q has been designed in several formulations for improving its pharmacokinetic limitations in recent years. Deformable-liposome conjugation with Q has been reported having many advantages, such as better stability and high solubility in HaCat cells [21]. Q deformable liposomes in UVB-irradiated cells also have shown to possess increased viability with decreased ROS and MDA. Other formulations, such as Q entrapped in glycerosomes and liposomes used on human keratinocytes in presence of H_2O_2 is shown to strengthen its antioxidant activity [39]. With the different proportions of Q, there has been up to 88–91 % efficiency and this has been incorporated into glycerosomes that proved to be carrying a higher antioxidant activity compared to pure Q forms. Q has also been coated with linoleic acid that influences reshaping of chitosan-oligosaccharides or β-lactoglobulin-nanoparticles that provide hydrophobicity, which is most desirable in the food industry [40].

We observed that $QTiO_2$ nano-antioxidants exhibited a high level of protection against ROS generation on mouse fibroblast cells (Fig. 6A). Severe and effective cell death occurred in the pure form of Q-treated

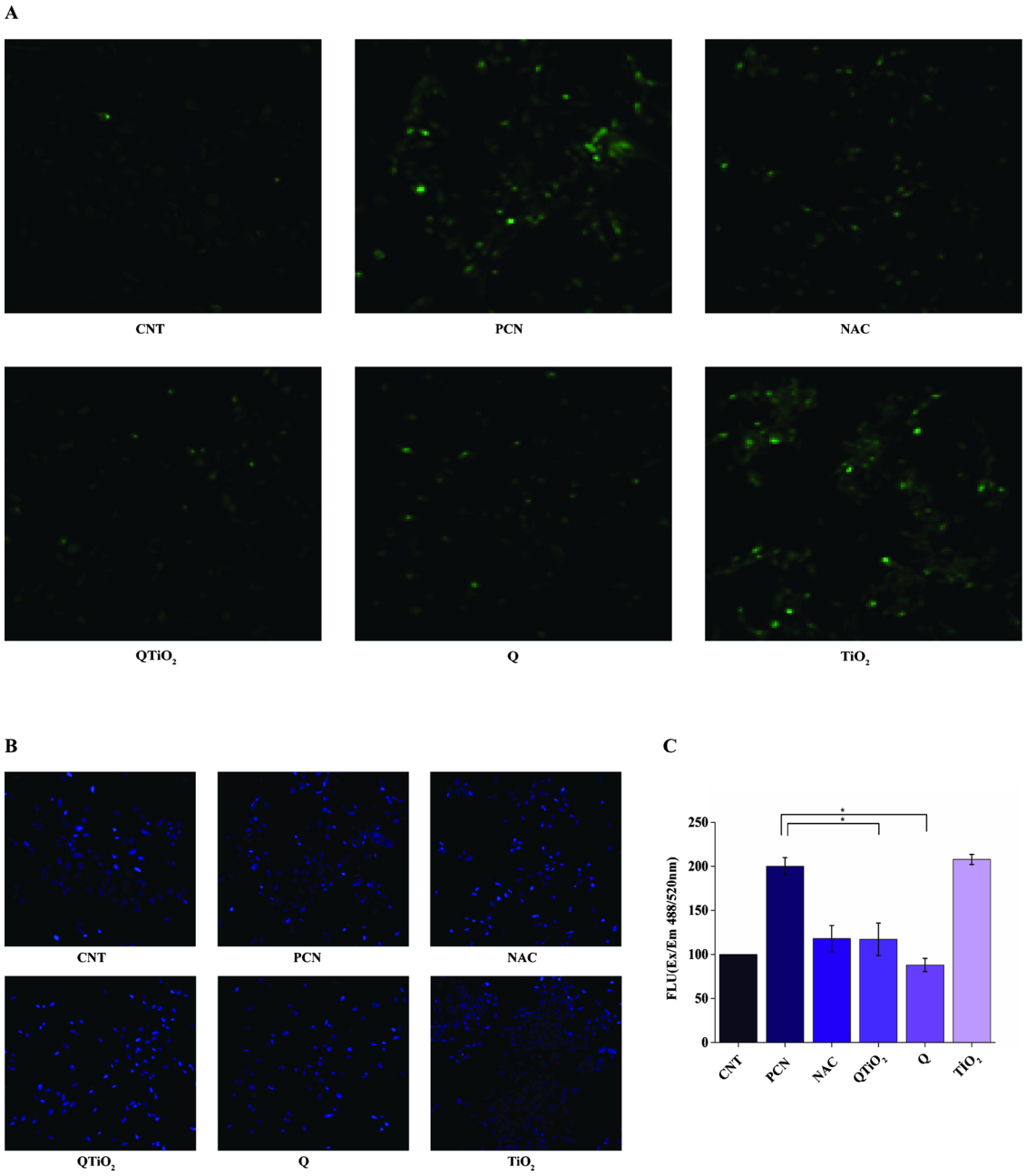

Fig. 7. Confocal microscopic examination of ROS in cells.
ROS screening was done by following manufacturer's kit protocol and PCN and NAC were used as inducer and inhibitor of ROS, respectively. **(A)** ROS level was scanned with green channel and represented as green color. **(B)** Cells nuclei were marked with dapi dye seen as blue color. **(C)** Confocal pictures were analysed by ImageJ software and cells dispersion per image were calculated by using particle analysis option of software. CTCF formulation was used for measurement fluorescence intensity per image then rounded off for 100 cells. Data state the mean results ± SEM, $n = 3$. *P $<$ 0.05 indicate a significant change between $QTiO_2$ and Q-treated cells compared to the positive control group.

cells and therefore, existence of the similar protective effect in cells as the ones treated with the $QTiO_2$ nano-antioxidant form was beyond comparison. Despite this difference, our results clearly implied that the designed nanosystem enabled safe cellular-delivery of high Q levels and therefore, Q tended to remain more stable and thereby enhancing the antioxidant potency, provided that is loaded on surface modified (PE-Gylated) TiO_2-nanoparticles. Further, quantitative ROS measurements were validated by laser scanning confocal microscopic screening (Fig. 7).

Bioenergetic events of cells are carried out by mitochondria and thus it is the major supplier of ROS, which is largely comprised of superoxide anions. Superoxide radicals are formed by electron leakage from respiratory chain complexes during oxidative phosphorylation [41]. Subsequently, the measured superoxide anion levels in our experimental model were similar with the total ROS levels (Fig. 6B). Protective effects of Q in the ROS formation, caused by mitochondrial dysfunction, have been reported in many studies. For example, Q has been shown to protect Caco-2 cells against mitochondrial damage [42]. In mouse zygotes, Q is shown to provide steady functional mitochondria by regulating cellular defence and reducing ROS [43]. In summary, 100 μg ml^{-1} of Q triggers mitochondrial dysfunction followed by cell death. However, the same amount of Q, if conjugated with PEG-functionalized TiO_2-nanoparticles, could provide a strong antioxidant property with no or negligible cytotoxicity (Fig. 6). The inherent

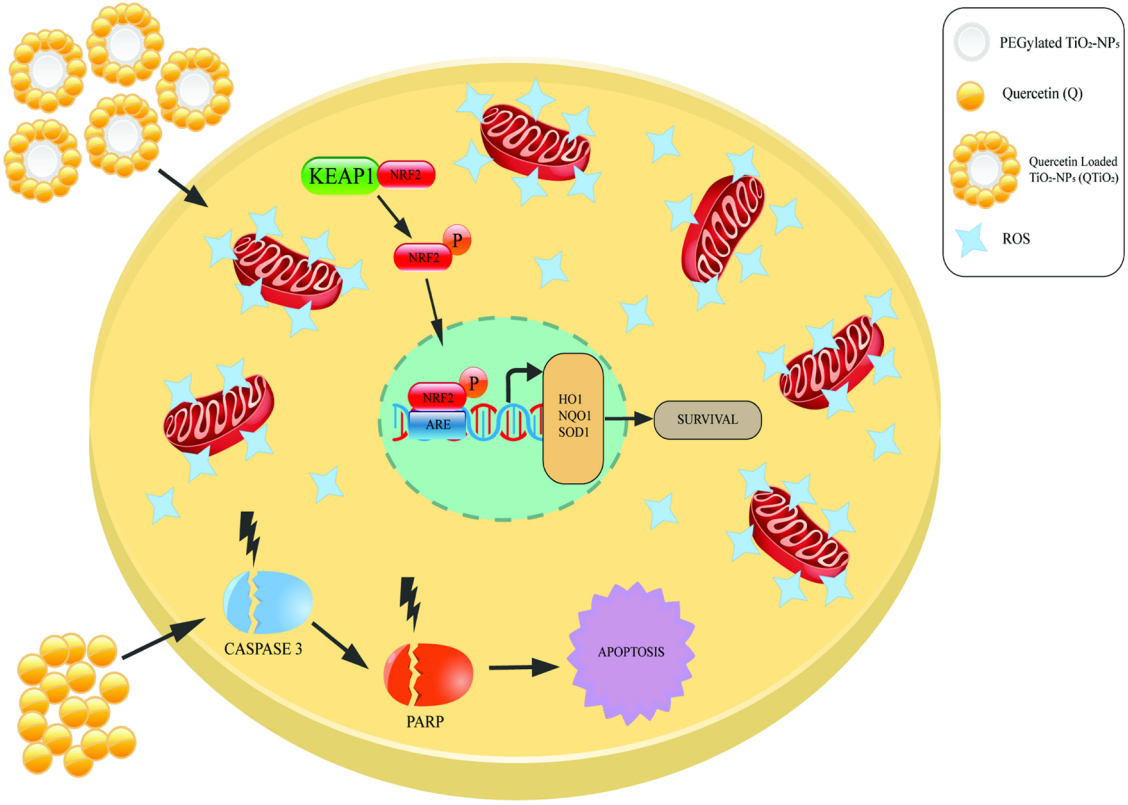

Fig. 8. Proposed illustration for biological effects of $QTiO_2$ nano-antioxidant and Q treatments on mouse fibroblast cells.

property of nano-sized TiO_2 along with Q does not only provide antioxidant-protection from oxidative skin-damage, but also forms a strong block against ultraviolet B exposure.

5. Conclusion

This study reports a novel nano-antioxidant design that is composed of PEGylated TiO_2-nanoparticles in which Q molecules are encapsulated. The nanosystem developed enabled maximum antioxidant properties for ROS and superoxide formation by keeping high Q levels, with stable functionality, in mouse fibroblast cells. Use of pure Q was toxic to cells, while with similar Q levels in the form of the $QTiO_2$-nanosystem it was found to have negligible or less-toxic effects. The $QTiO_2$ nano-antioxidant provided to be an effective intercellular Q delivery system with no obvious cytotoxic effects, resulting in the $QTiO_2$ system to be a promising carrier for Q molecules. The $QTiO_2$ nano-antioxidant formulation can be used in topical creams as a therapeutic agent for improving cellular defence for oxidative toxicity, ultraviolet-damage and inflammation.

Author contributions

Yelda Birinci
Conceived and designed the analysis, Collected the data, Contributed data or analysis tools, Performed the analysis, Wrote the paper, Manuscript editing
Javed H. Niazi
Performed the analysis
Oznur Aktay-Cetin
Performed the analysis, RNA assay, Colocalization analysis
SEM analysis, FTIR and Fluorescence Spectra Profiling, Wrote the paper
Manuscript editing.
Huveyda Basaga
Conceived and designed the analysis, Wrote the paper
Manuscript editing.
Birinci Y_ Author Agreement

Declaration of Competing Interest

No potential conflict of interest was reported by the authors.

Acknowledgement

The authors would like to thank Prof. Mehmet Ali Gulgun for the SEM images of $QTiO_2$, Talat Hussain Khan for the illustration of Q and $QTiO_2$ biological effects on survival mechanism in mouse fibroblast cells, and also to Dr. Christopher Mayack for the English editing.

Appendix A. Supplementary data

Supplementary material related to this article can be found, in the online version, at doi:https://doi.org/10.1016/j.enzmictec.2020.109559.

References

[1] P.A. Mouthuy, S.J. Snelling, S.G. Dakin, L. Milkovic, A.C. Gasparovic, A.J. Carr, N. Zarkovic, Biocompatibility of implantable materials: an oxidative stress viewpoint, Biomaterials 109 (2016) 55–68.
[2] J. Mierziak, W. Wojtasik, K. Kostyn, T. Czuj, J. Szopa, A. Kulma, Crossbreeding of transgenic flax plants overproducing flavonoids and glucosyltransferase results in progeny with improved antifungal and antioxidative properties, Mol. Breed. 34 (4) (2014) 1917–1932.
[3] I. Morel, G. Lescoat, P. Cogrel, O. Sergent, N. Pasdeloup, P. Brissot, P. Cillard, J. Cillard, Antioxidant and iron-chelating activities of the flavonoids catechin, quercetin and diosmetin on iron-loaded rat hepatocyte cultures, Biochem. Pharmacol. 45 (1) (1993) 13–19.
[4] L. Chebil, C. Humeau, J. Anthoni, F. Dehez, J.M. Engasser, M. Ghoul, Solubility of flavonoids in organic solvents, J. Chem. Eng. Data 52 (5) (2007) 1552–1556.
[5] T. Hatahet, M. Morille, A. Hommoss, J.M. Devoisselle, R.H. Muller Begu, Quercetin

topical application, from conventional dosage forms to nanodosage forms, Eur. J. Pharm. Biopharm. (2016).
[6] R. Vago, V. Collico, S. Zuppone, D. Prosperi, M. Colombo, Nanoparticle-mediated delivery of suicide genes in cancer therapy, Pharmacol. Res. 111 (2016) 619–641.
[7] J.L. Chen, W.E. Fayerweather, Epidemiologic study of workers exposed to titanium dioxide, Journal of occupational medicine, official publication of the Industrial Medical Association 30 (12) (1988) 937–942.
[8] B.K. Bernard, M.R. Osheroff, A. Hofmann, J.H. Mennear, Toxicology and carcinogenesis studies of dietary titanium dioxide-coated mica in male and female Fischer 344 rats, J. Toxicol. Environ. Health 29 (4) (1990) 417–429.
[9] G.A. Hart, T.W. Hesterberg, In vitro toxicity of respirable-size particles of diatomaceous earth and crystalline silica compared with asbestos and titanium dioxide, J. occupational and environmental medicine / American College of Occupational and Environmental Medicine 40 (1) (1998) 29–42.
[10] F.P. Gasparro, M. Mitchnick, J.F. Nash, A review of sunscreen safety and efficacy, Photochem. Photobiol. 68 (3) (1998) 243–256.
[11] M. Jarosz, A. Pawlik, M. Szuwarzynski, M. Jaskula, G.D. Sulka, Nanoporous anodic titanium dioxide layers as potential drug delivery systems: drug release kinetics and mechanism, Colloids Surf. B Biointerfaces 143 (2016) 447–454.
[12] G. Devanand Venkatasubbu, S. Ramasamy, V. Ramakrishnan, J. Kumar, Folate targeted PEGylated titanium dioxide nanoparticles as a nanocarrier for targeted paclitaxel drug delivery, Adv. Powder Technol. 24 (6) (2013) 947–954.
[13] A.P. Nifli, P.A. Theodoropoulos, S. Munier, C. Castagnino, E. Roussakis, H.E. Katerinopoulos, J. Vercauteren, E. Castanas, Quercetin exhibits a specific fluorescence in cellular milieu: a valuable tool for the study of its intracellular distribution, J. Agric. Food Chem. 55 (8) (2007) 2873–2878.
[14] I. Baran, E. Katona, C. Ganea, Quercetin as a fluorescent probe for the ryanodine receptor activity in Jurkat cells, Pflugers Arch. 465 (8) (2013) 1101–1119.
[15] K.J. Livak, T.D. Schmittgen, Analysis of relative gene expression data using real-time quantitative PCR and the $2-\Delta\Delta CT$ method, Methods 25 (4) (2001) 402–408.
[16] V. Zinchuk, O. Zinchuk, Quantitative colocalization analysis of confocal fluorescence microscopy images, Curr. Protoc. Cell Biol. 39 (1) (2008) 4.19.1-4.19.16..
[17] E. Amanzadeh, A. Esmaeili, R.E.N. Abadi, N. Kazemipour, Z. Pahlevanneshan, S. Beheshti, Quercetin conjugated with superparamagnetic iron oxide nanoparticles improves learning and memory better than free quercetin via interacting with proteins involved in LTP, Sci. Rep. 9 (1) (2019) 6876.
[18] A.R.T. Kelly, E. Heim, Dennis J. Bobilya, Flavonoid antioxidants: chemistry, metabolism and structure-activity relationships, Journal of Nutritional Biochemistry 13 572–584.
[19] B.W.M.C.S. M, Flavonoid antioxidants: rate constants for reactions with oxygen radicals, Meth. Enzymol. (1994) 420–429. Academic Press.
[20] Q. Tan, W. Liu, C. Guo, G. Zhai, Preparation and evaluation of quercetin-loaded lecithin-chitosan nanoparticles for topical delivery, Int. J. Nanomedicine 6 (2011) 1621–1630.
[21] D. Liu, H. Hu, Z. Lin, D. Chen, Y. Zhu, S. Hou, X. Shi, Quercetin deformable liposome: preparation and efficacy against ultraviolet B induced skin damages in vitro and in vivo, J. Photochem. Photobiol. B 127 (2013) 8–17.
[22] Z. Chen, Y. Wang, T. Ba, Y. Li, J. Pu, T. Chen, Y. Song, Y. Gu, Q. Qian, J. Yang, G. Jia, Genotoxic evaluation of titanium dioxide nanoparticles in vivo and in vitro, Toxicol. Lett. 226 (3) (2014) 314–319.
[23] K. Niska, K. Pyszka, C. Tukaj, M. Wozniak, M.W. Radomski, I. Inkielewicz-Stepniak, Titanium dioxide nanoparticles enhance production of superoxide anion and alter the antioxidant system in human osteoblast cells, Int. J. Nanomedicine 10 (2015) 1095–1107.
[24] S.M. Hussain, K.L. Hess, J.M. Gearhart, K.T. Geiss, J.J. Schlager, In vitro toxicity of nanoparticles in BRL 3A rat liver cells, Toxicol. In Vitro 19 (7) (2005) 975–983.
[25] E. Dickancaite, A. Nemeikaite, A. Kalvelyte, N. Cenas, Prooxidant character of flavonoid cytotoxicity: structure-activity relationships, Biochem. Mol. Biol. Int. 45 (5) (1998) 923–930.
[26] I.K. Wang, S.Y. Lin-Shiau, J.K. Lin, Induction of apoptosis by apigenin and related flavonoids through cytochrome c release and activation of caspase-9 and caspase-3 in leukaemia HL-60 cells, Eur. J. Cancer 35 (10) (1999) 1517–1525.
[27] Guohua Cao, a.R.L.P. Emin Sofic, Antioxidant and prooxidant behavior of flavonoids:structure-activity relationships, Free Radic. Biol. Med. 22 (1997).
[28] M. Nagao, N. Morita, T. Yahagi, M. Shimizu, M. Kuroyanagi, M. Fukuoka, K. Yoshihira, S. Natori, T. Fujino, T. Sugimura, Mutagenicities of 61 flavonoids and 11 related compounds, Environ. Mutagen. 3 (4) (1981) 401–419.
[29] C.A. Elliger, P.R. Henika, J.T. MacGregor, Mutagenicity of flavones, chromones and acetophenones in Salmonella typhimurium. New structure-activity relationships, Mutat. Res. 135 (2) (1984) 77–86.
[30] S. Elmore, Apoptosis: a review of programmed cell death, Toxicol. Pathol. 35 (4) (2007) 495–516.
[31] C. Assuncao Guimaraes, R. Linden, Programmed cell deaths. Apoptosis and alternative deathstyles, Eur. J. Biochem. 271 (9) (2004) 1638–1650.
[32] H.R. Stennicke, G.S. Salvesen, Caspases - controlling intracellular signals by protease zymogen activation, Biochim. Biophys. Acta 1477 (1-2) (2000) 299–306.
[33] K.C. Liu, C.Y. Yen, R.S. Wu, J.S. Yang, H.F. Lu, K.W. Lu, C. Lo, H.Y. Chen, N.Y. Tang, C.C. Wu, J.G. Chung, The roles of endoplasmic reticulum stress and mitochondrial apoptotic signaling pathway in quercetin-mediated cell death of human prostate cancer PC-3 cells, Environ. Toxicol. 29 (4) (2014) 428–439.
[34] S.Y. Chien, Y.C. Wu, J.G. Chung, J.S. Yang, H.F. Lu, M.F. Tsou, W.G. Wood, S.J. Kuo, D.R. Chen, Quercetin-induced apoptosis acts through mitochondrial- and caspase-3-dependent pathways in human breast cancer MDA-MB-231 cells, Hum. Exp. Toxicol. 28 (8) (2009) 493–503.
[35] L. He, X. Hou, F. Fan, H. Wu, Quercetin stimulates mitochondrial apoptosis dependent on activation of endoplasmic reticulum stress in hepatic stellate cells, Pharm Biol (2016) 1–10.
[36] D. Metodiewa, A.K. Jaiswal, N. Cenas, E. Dickancaite, J. Segura-Aguilar, Quercetin may act as a cytotoxic prooxidant after its metabolic activation to semiquinone and quinoidal product, Free Radic. Biol. Med. 26 (1-2) (1999) 107–116.
[37] T. Nguyen, C.S. Yang, C.B. Pickett, The pathways and molecular mechanisms regulating Nrf2 activation in response to chemical stress, Free Radic. Biol. Med. 37 (4) (2004) 433–441.
[38] S.J. Kang, B.M. Kim, Y.J. Lee, S.H. Hong, H.W. Chung, Titanium dioxide nanoparticles induce apoptosis through the JNK/p38-caspase-8-Bid pathway in phytohemagglutinin-stimulated human lymphocytes, Biochem. Biophys. Res. Commun. 386 (4) (2009) 682–687.
[39] M.L. Manca, I. Castangia, C. Caddeo, D. Pando, E. Escribano, D. Valenti, S. Lampis, M. Zaru, A.M. Fadda, M. Manconi, Improvement of quercetin protective effect against oxidative stress skin damages by incorporation in nanovesicles, Colloids Surf. B Biointerfaces 123 (2014) 566–574.
[40] Y. Zhao, J.L. Howe, Z. Yu, D.T. Leong, J.J. Chu, J.S. Loo, K.W. Ng, Exposure to titanium dioxide nanoparticles induces autophagy in primary human keratinocytes, Small 9 (3) (2013) 387–392.
[41] G. Lenaz, The mitochondrial production of reactive oxygen species: mechanisms and implications in human pathology, IUBMB Life 52 (3-5) (2001) 159–164.
[42] C. Carrasco-Pozo, M.L. Mizgier, H. Speisky, M. Gotteland, Differential protective effects of quercetin, resveratrol, rutin and epigallocatechin gallate against mitochondrial dysfunction induced by indomethacin in Caco-2 cells, Chem. Biol. Interact. 195 (3) (2012) 199–205.
[43] S. Yu, H. Long, Q.F. Lyu, Q.H. Zhang, Z.G. Yan, H.X. Liang, W.R. Chai, Z. Yan, Y.P. Kuang, C. Qi, Protective effect of quercetin on the development of pre-implantation mouse embryos against hydrogen peroxide-induced oxidative injury, PLoS One 9 (2) (2014) e89520.